ISSN 1070-3632, Russian Journal of General Chemistry, 2014, Vol. 84, No. 1, pp. 25–32. © Pleiades Publishing, Ltd., 2014.
Original Russian Text © V.V. Korochentsev, I.S. Os'mushko, I.B. Lvov, A.A. Komissarov, A.A. Dotsenko, T.V. Sedakova, A.G. Mirochnik, V.I. Vovna, 2014, published in Zhurnal Obshchei Khimii, 2014, Vol. 84, No. 1, pp. 27–34.

Electronic Structure of Guanidine and Its Derivatives from X-ray Photoelectron Spectroscopy and Density Functional Theory Studies

V. V. Korochentsev[a], I. S. Os'mushko[a], I. B. Lvov[a], A. A. Komissarov[a], A. A. Dotsenko[a], T. V. Sedakova[b], A. G. Mirochnik[b], and V. I. Vovna[a]

[a] *Far Eastern Federal University, ul. Sukhanova 8, Vladivostok, 690950 Russia*
e-mail: korochen@vido.dvgu.ru

[b] *Institute of Chemistry, Far East Branch, Russian Academy of Sciences, Vladivostok, Russia*

Received January 14, 2013

Abstract—Electronic structure of guanidine, diphenylguanidine, their protonated forms, and guanidinium chloride have been studied by X-ray photoelectron spectroscopy and quantum-chemical modeling. From the derived geometry parameters and electronic structure, the effect of protonation on localization of the electron density has been revealed. The lines in the valence region of the X-ray photoelectron spectra have been assigned.

DOI: 10.1134/S1070363214010071

Experimental and theoretical studies of several new luminescent and chromogenic complexes of lanthanides and *p*-elements, including Sb(III) and Te(IV) complexes, have revealed the mechanisms of the related photochemical processes and structural changes, and have established the relationship between the compound electronic structure and its physicochemical properties (reactivity, photostability, thermal stability, and luminescence intensity) [1, 2]. Thus, the optical properties of the complexes and the derived light-transforming polymer materials can be efficiently regulated.

Guanidinium and *N*,*N*'-diphenylguanidinium salts are widely used in industrial production of plastics, propellants, surfactants, fillers, resins, antibacterial and antiviral polymeric materials [3]. Complex compounds of Sb(III) and Te(IV) with guanidine and diphenylguanidine possess unique luminescent and optical properties, in particular, Sb(III) complexes have shown enhanced photostability and intense luminescence at room temperature, furthermore, they may act as actuators for light-transforming polymer materials. Te (IV) compounds are known for thermochromic behavior and thus can be used in temperature indicators [4]. As is known, luminescence of such complexes can arise from the transfer of electronic excitation energy from the diphenylguanidine ion to Sb(III) and Te(IV) ones [4]. The role of the ligand–metal, metal–ligand and ligand–ligand charge transfer in photophysical properties of the coordination compounds have been studied by altering the donor-acceptor properties of the ligands and the charge state of the ions [5]. However, the important information on the electronic structure of the guanidine and guanidinium compounds has been scarce so far.

In this work, we used X-ray photoelectron spectroscopy and quantum chemistry methods to study the electronic structure of guanidine (**I**), diphenylguanidine (**IV**), their protonated forms (**II** and **V**, respectively), and guanidinium chloride (**III**). We report on their electronic structure, localization of the electron density, and the effect of protonation on the electronic structure. The valence region bands in X-ray photoelectron spectra of **III** and **IV** have been assigned**.**

According to the calculations, compounds **I**, **IV,** and **V** contained a planar CN_3 fragment. In **I,** the highest deviation of the amine N^2–H hydrogen atom from the CN_3 plane was of 40°, and the N^3–H hydrogen deviated by 35° to the other side of CN_3 plane. The CN^2HR fragment was nearly tetrahedral: the sum of the three angles at the amine atoms was of 340°. In **IV,** angle between the phenyl rings was of 52°.

Table 1. Localization of the electron density at the atoms of compounds **I–V**, %

Atom, Group of atoms	Compound **I**								
NMO(type)	16(π_3)	15(n_N)	14(π_2)	13(π_1)	12(σ)	11(σ)	10(σ)	9(σ)	8(σ)
C	9	12	3	35	20	12	8	15	23
N^1–H	54	76	6	17	32	14	8	21	12
2(NH_2)	37	12	91	54	48	74	84	64	65
	Compound **II**								
Orbital	16(π_3)	15(π_2)	14(π_1)	13(σ)	12(σ)	11(σ)	10(σ)	9(σ)	8(σ)
C	3	3	36	14	14	4	17	17	21
NH_2		64	21	35	23	22	24	30	26
2(NH_2)	97	33	43	51	63	74	59	53	53
	Compound **III**								
Orbital	22(π_3)	21(π_2)	20(π)	19(π_1)	18(σ)	17(σ)	16(σ)	15(σ)	14(σ)
C	4	3	37	14	2	20	10	19	11
(NH_2)	0	64	24	17	10	30	58	25	13
2(NH_2)	96	33	39	64	87	50	32	61	34
Cl[a]	0	0	0	5	1	0	0	5	42
	Compound **IV**								
Orbital	56(π)	55(π)	54(π)	53(π)	52(σ)	51(π)	50(π)	49(σ)	48(σ)
C	2	2	0	2	6	10	0	0	0
(N–H)	9	17	0	17	55	27	0	3	0
2(NH)	25	27	0	1	4	10	37	1	1
2(Ph)	64	54	100	80	35	53	63	96	99
	Compound **V**								
Orbital	56(π)	55(π)	54(π)	53(π)	52(π)	51(π)	50(σ)	49(σ)	48(σ)
C	0	0	1	0	3	3	1	0	
(NH_2)	1	0	0	1	0	54	7	0	
2(NH)	0	0	0	3	75	30	2	10	4
2(Ph)	100	100	100	96	22	13	90	90	96

[a] The three highest Cl3*p* orbitals are not shown.

The sequence of the HOMOs of **I** (π_3, n_N, π_2, and π_1) is shown in Fig. 1; the contributions of the atoms, including C, HN and two NH_2 groups, to the valence MOs are collected in Table 1.

From the calculated electronic structure of **II,** significant stabilization of all its orbitals (~6.75 eV) as compared to the corresponding orbitals of compound **I** was revealed. For the clarity, the HOMO of **II** (π_3) was shifted to be equal in energy to the HOMO of **I** (π_3). Therefore, all the MOs energies in **II** were increased by 6.75 eV in the correlation diagram (Fig. 1).

As compared with **I,** the strongest stabilization of MO in **II** was observed in the case of the n_N orbital (no. 15), with 88% of the electron density being

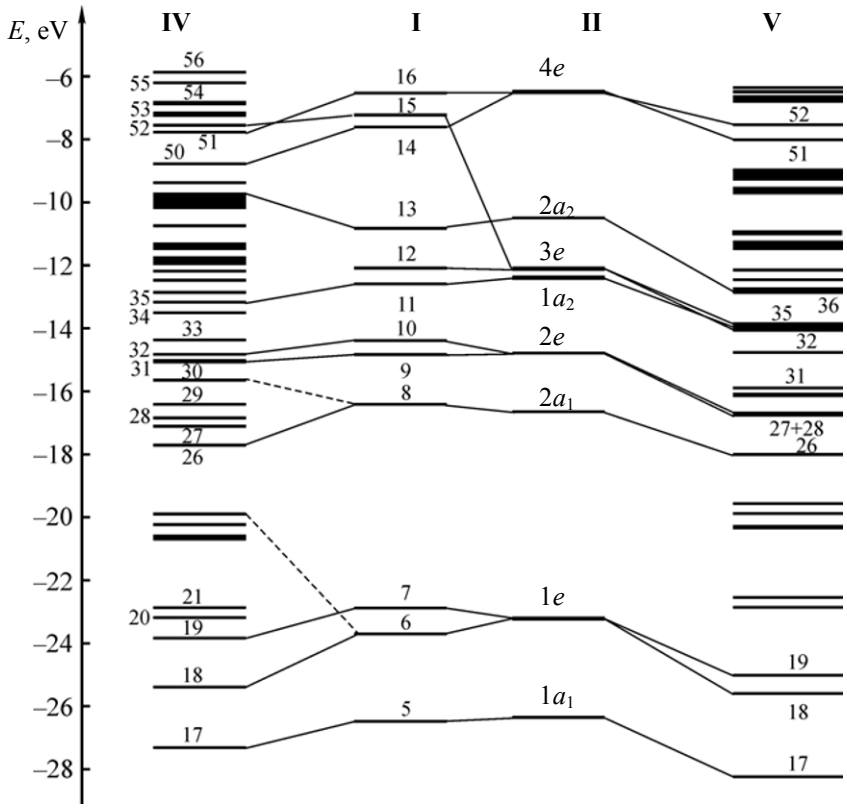

Fig. 1. Correlation diagram of the molecular orbitals.

localized at the C atom and at N^1–H group. In the case of the carbon atom, the contribution of 2*s* orbitals was of 20% and that of 2*p* orbitals was of 50%.

In guanidinium chloride **III,** the influence of halogen and positively charged hydrogen atom led to stabilization of all the orbitals; due to redistribution of the electron density, the MO sequence changed. The three highest orbitals were localized at the chlorine atom, then the π_3, π_2, and π_1 orbitals followed (Table 2). Localization of the strongly stabilized n_N orbitals at the CN^1H fragment was reduced to 12% due to the effect of positively charged hydrogen atom; the electron density was redistributed at the amine groups (87%). The stabilization energy ranged from 1.29 eV (π_2 orbitals) to 6.84 eV (n_N).

From the computations results and taking into account the contributions of Cl^- to the guanidinium cation orbitals, we concluded that the HGu^+–Cl^- bond was ionic, and the main causes the MOs energy changes were the field effect and the redistribution of electron density from the proton to the guanidine fragment atoms.

The valence MOs of **IV** included the orbitals localized predominantly at the atoms of central part of the molecule (guanidine fragment) (more than 80%), those localized at the atoms of the phenyl rings (more than 90%), and the mixed orbitals, with the contribution of the guanidine fragment atoms being of over 30% that of the phenyl fragments being of over 50%. The four highest occupied MOs of **IV** were π orbitals localized predominantly at the atoms of phenyl rings (Table 1).

The HOMO of **V** was equated in energy to the HOMO of **I** for clarity; thus, all the energies of MOs in **V** were increased by 3.9 eV. Stabilization and the energy order changes of the highest occupied levels in **V** were mainly due to the redistribution of the electron

Table 2. The binding energy and the lines half-width corresponding to C and N atoms of **IV**

Electrons	E_b, eV	Half-width, eV
C1*s* (Ph)	284.9	1.6
C1*s* (C–N)	286.2	1.6
C1*s* (3N)	288.3	1.6
N1*s*	400.1	1.7
N1*s* (NH)	398.4	1.7

density at the atoms upon addition of H^+. The most stabilized MOs were those localized at the nitrogen atoms and at the central carbon atom (by 4.65 eV at the average). The lowest stabilization occurred in the case of MOs localized at Ph rings (3.53 eV at the average). For the mixed orbitals, the stabilization effect was somewhat in between (about 4.3 eV).

The four highest MOs of **V** were localized at Ph rings almost completely (Table 1), the next two orbitals (π_3 and π_2) were mixed MO localized at the guanidine fragment atoms by 78% and 87%, respectively.

Figure 2 presents an overview of X-ray photoelectron spectrum of **IV** along with the detailed spectra of 1*s* electrons of C and N and of the valence region. The overview spectrum contained the bands of Auger transitions as well as the 1*s* electrons lines, the intensity of the latter being determined by the empirical formula of the sample and the relative ionization cross-section of the levels. The binding energies E_b and the respective band half-widths are listed in Table 2.

The C1*s* line consisted of the three basic components: the most intense one with maximum at

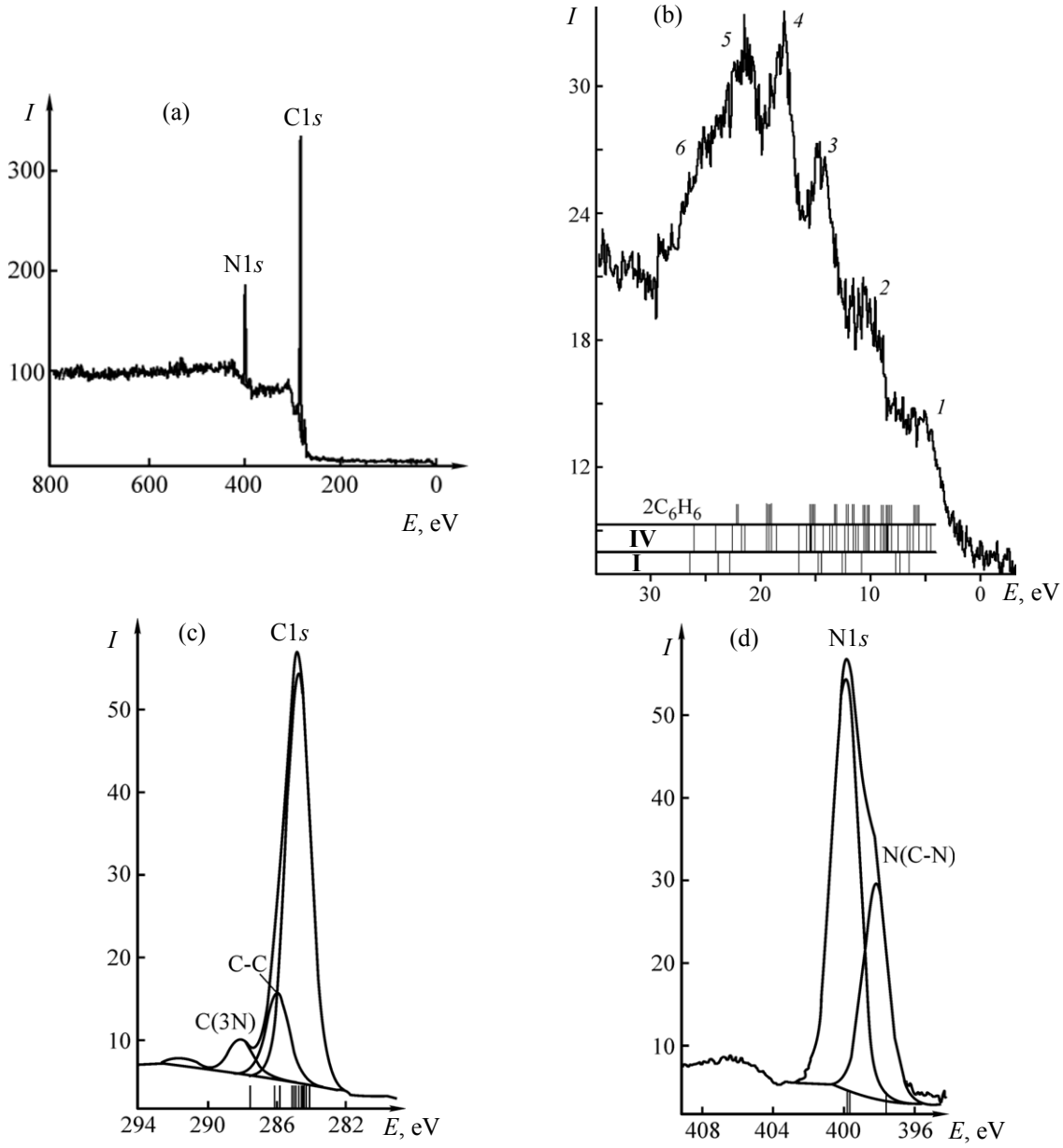

Fig. 2. General view of the spectrum of **IV** (a); the extended views of the valence region (b) and of the regions of 1*s* level of C (c) and N (d).

284.9 eV referred to the carbon atoms of phenyl rings, two other components were assigned to the carbon atoms of phenyl rings connected with the nitrogen atom (C–N) and to the carbon atoms surrounded by three nitrogen atoms CN_3. The weak peak at 291–292 eV confirmed the C1s band assignment; it originated from the shake-up effect: the electron knocked out from the deeper level excited another one (usually from the valence π-orbital) and thus lose part of the kinetic energy [7]. In the case of **IV**, the corresponding energy was of 6.5 eV

The N1*s* line (Fig. 2d) clearly included two components with the intensity ratio of 2 : 1, corresponding to the two states of nitrogen: the two N atoms bound to the central and to the phenyl carbon atoms, and the amine nitrogen. The experimentally determined splitting energy of N1*s* level was of 1.7 eV, being in good correspondence with the calculated value.

Upon transition to the condensed phase, the subzones of MOs were formed in the valence region of the spectrum (Fig. 2b), mainly of π- and σ-levels of *p*-type and of the levels with the dominant contribution from 2*s*-orbitals of carbon and nitrogen. In the overlapping bands, six peaks were identified, nicely correlating with the calculated MOs. As the bands intensities were determined by the ionization cross-sections as well as by the density of states, the most intense bands were the three bands in the region of the *s*-levels ionization.

The valence levels could be assigned basing on the quantum-chemical computations and the spectral curve deconvolution. In Fig. 2, the calculated energies are shown overlaid in the valence region spectrum. The highest occupied MOs of **IV** were π-orbitals, the contribution of guanidine fragment to the two upper MOs being of 36 and 46%, respectively. The third MO was by 99% localized at the phenyl fragment. The mentioned MOs contributed to the first broad band of the spectrum. The orbitals below the eighth one belonged to phenyl fragment and corresponded to the second band of the spectrum. The third band contained the contributions of the six electron pairs of guanidine (π-type) and phenyls (σ-type, C2*p*). The four phenyl pairs contributed to the fourth band with the energy of 17.5 eV. The sixth band was due to the three electron pairs of N atoms, and the fifth band was due to the five C2*s* levels.

The above-described assignment was confirmed by the computation results as well as by the correlation of the photoionization cross-sections of nitrogen (almost two times higher than that of C2*s* [7, 14]). The width of the calculated valence band coincided with the experimental one (Fig. 2d).

Table 3. The binding energy and the lines half-width corresponding to C, O, N, Cl atoms of **III**

Electrons	E_b, eV	Half-width, eV
C1*s*	285.0	1.7
C1*s*(3N)	289.3	1.5
O1*s*	532.1	2.1
N1*s*	400.1	1.7
Cl2*p*2p$_{3/2}$	198.0	1.5
Cl2*p*2p$_{1/2}$	199.7	1.8

The X-ray photoelectron spectrum of **III** is shown in Fig. 3. The corresponding E_b and half-width values are collected in Table 3.

In the general view, a weak line of oxygen was observed along with the expected lines of the core levels of C, N, and Cl. In the C1*s* sub-spectrum, the band at 289.3 eV was assigned to the central carbon atom with the effective charge of 0.22 *e* (calculated). The stronger carbon band at 285.0 eV corresponded to the impurities in the reaction product. The three equivalent nitrogen atoms of the NH_2 groups were assigned to the only band with half-width of 1.7 eV (Table 3). The Cl2*p* line consisted of two bands ($2p_{1/2}$ and $2p_{3/2}$), the spacing between them being of 1.7 eV, with almost equal half-widths and the intensity ratio of 1:1.5. The energy of Cl2$p_{1/2}$ line was of 199.7 eV, the shift to lower energy was due to the negative charge on chlorine atom.

The nitrogen E_b value was of 400.1 eV, typical of NH_2 groups in inorganic compounds; the chlorine E_b value was common for the transition metal chlorides with highly ionic bonds.

In order to interpret the spectrum of valence electrons (Fig. 3b), we considered the computed electronic structure of **III**. Under approximation of the planar $C(NH_2)_3^+$ group and not considering the effect of chlorine atom on the structure, the D_{3h} symmetry group was suggested. In view of the symmetry, the four non-degenerate and four doubly degenerate MOs were occupied. According to the computation results, the sequence of the occupied MOs in the free cation was as follows: $1a_1'$, $1e'$, $2a_1'$, $2e'$, $3e'$, $1a_2'$, $1a_2''$, $1e''$.

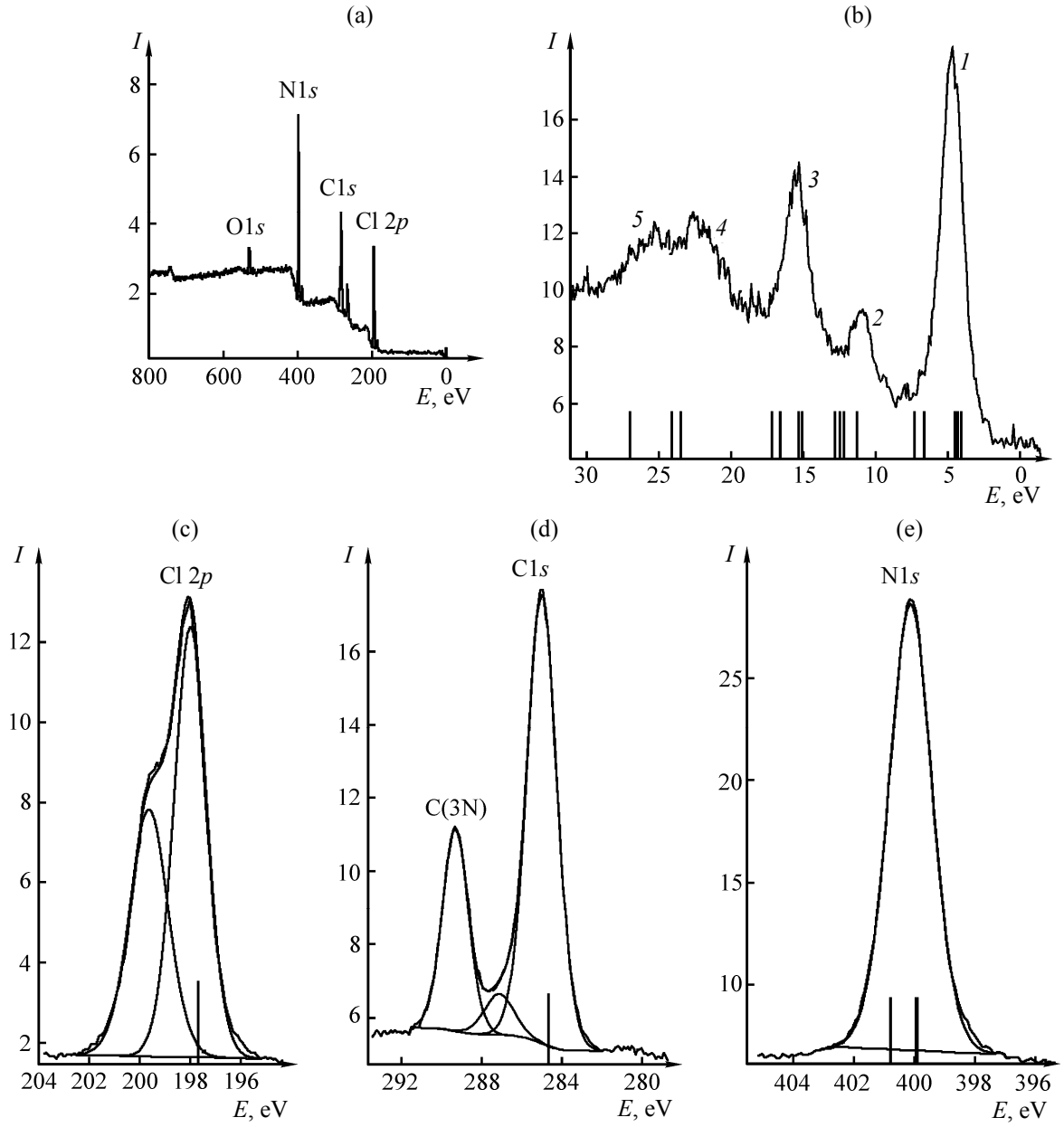

Fig. 3. General view of the spectrum of **III** (a); the extended views of the valence region (b) and of the regions of 1*s* level of Cl (c), C (d), and N (e).

The 2*s* AOs of carbon and nitrogen predominantly contributed to the three lowest levels; the two highest π-type levels were localized at the four central atoms; the other three σ-type MOs formed the C–N and N–H bonds. The chlorine atom was bound to the two H atoms via hydrogen bonding and therefore lowered the complex symmetry to C_{2v} and eliminated the degeneracy of *e*-MOs. Three electron pairs of chlorine occupied the levels above any of the guanidinium cation levels.

The first (strong) band in the valence levels spectrum corresponded to the Cl3*p* and to the 1*e*"(π) electrons of the cation. The second (weak) band at 11 eV was due to binding levels correlating with the $3e'\ 1a_2'\ 1a_2''$ MOs of the free cation. The third (strong) band was assigned to the $2a_2'$ and $2e'$ MOs with the chlorine 3*s* MO located between them. The high ionization energy of the latter led to the difference in the intensities of the second and the third bands. Finally, according to the modeling, the forth band was

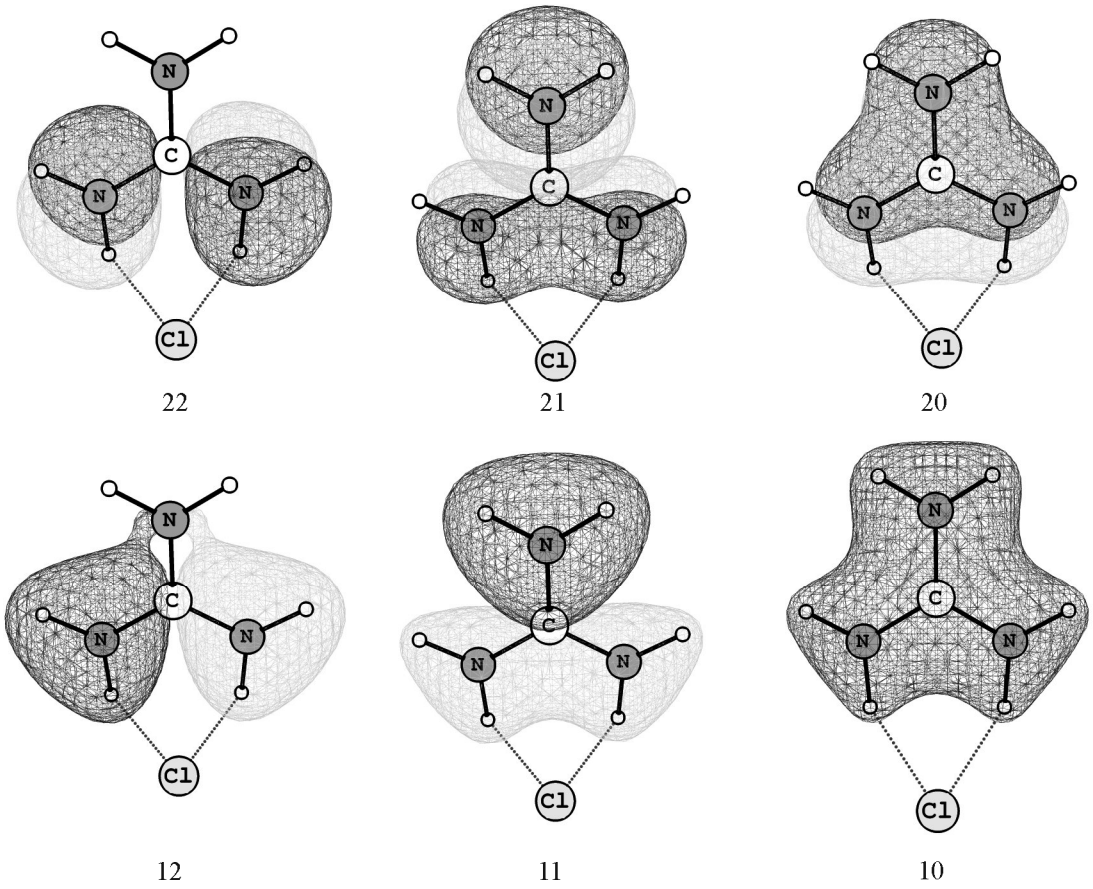

Fig. 4. Localization of electron density at the molecular orbitals of **III.**

assigned to two close nitrogen 2*s* levels and the fifth band was assigned to the lower of the 2*s* valence nitrogen levels (orbitals 10, 11, 12 in Fig. 4).

To conclude, the X-ray photoelectron spectroscopy and quantum chemistry studies of guanidine and some of its derivatives revealed that the change in the energy of the valence orbitals was due to the field effect. The concentrations of elements in guanidinium chloride and diphenylguanidine derivatives were determined. Basing on the quantum-chemical modeling, the valence bands in the X-ray photoelectron spectra were assigned.

EXPERIMENTAL

X-ray photoelectron spectra were registered with ultrahigh vacuum photoelectron spectrometer Omicron (Germany) equipped with a hemispherical electrostatic analyzer (curvature radius of 125 mm). The X-ray source was equipped the magnesium anode (MgK_α line of 1253.6 eV).

The spectral regions corresponding to the O1*s*, C1*s*, N1*s*, and Cl2*p* atomic levels were recorded at the analyzer transmittance energy of 20 eV. The instrumental function at that mode (as determined from the by shape of the Ag3$d_{5/2}$ line) revealed a half-width of 1.2 eV. The general spectrum including all the characteristic lines was recorded at the energy of 50 eV.

The chamber pressure did not exceed 9×10^{-12} bar. During the signal accumulation, the lines parameters did not change, thus indicating the stationary sample composition and surface state as well as the constant induced effective charge.

The spectra were processed using the CASA XPS software [6]. The energy scale was calibrated using the C1*s* internal reference. The binding energy of C1*s* electrons in **IV** was of 294.9 eV [7]. In the case of **III**, the C1*s* band of the residual solvent, 285 eV, was chosen as the reference. The atoms chemical state was analyzed by deconvolution of the spectral lines into

combinations of Gaussian and Lorentz bands. Quantitative analysis was performed with accounting for the photoionization cross-sections and the dependence of the mean free path of electrons in a sample on their speed [8]. The reproducibility of triplicate E_b measurements was within 0.1 eV

Quantum-chemical modeling was performed in the frame of density functional theory [9] using the Firefly software package [10]. We used the B3LYP5 hybrid exchange-correlation functional [11]. Optimization of **I–III** geometry was performed in the TZVPP [12–14] basis. Compounds **IV** and **V** were modeled in the 6-31G and TZVPP basis sets (in the latter basis, the geometry optimization was skipped being extremely time-consuming; instead, the geometry optimized in the 6-31G basis was used). The correspondence of the optimized structures to local minima of the potential energy surface was confirmed by calculation of the Hessian.

REFERENCES

1. Vogler, A. and Kunkely, H., *Coord. Chem. Rev*., 1998, vol. 177, p. 81
2. Guillaumont, D. and Daniel, C., *Coord. Chem. Rev.,* 1998, vol. 177, p. 181
3. Afinogenov, G.E. and Panarin, E. F., *Antimikrobnye polimery* (Antimicrobial Polymers), St. Petersburg: Gippokrat, 1993.
4. Mirochnik, A.G., *Doctoral (Chem.) Dissertation*, Vladivostok, 2007.
5. Balzani, V., Credi, A., and Venturi, M., *Coord. Chem. Rev*., 1998, vol. 177, p. 3
6. *CASA XPS Version 2.3.12*, Casa Software Ltd., 1999–2006.
7. Nefedov, V.I. and Vovna, V.I., *Elektronnaya struktura organicheskikh i elementoorganicheskikh soedinenii* (Electronic Structure of Organic and Organometallic Compounds), Moscow: Nauka, 1989.
8. Karlsson, T. A., *Fotoelektronnaya i Ozhe-spektroskopiya* (Photoelectron and Auger Spectroscopy), Leningrad: Mashinostroenie, 1981.
9. Parr, R. and Yang, W., *Density-Functional Theory of Atoms and Molecules*, New York: Oxford University Press, 1989.
10. Granovsky, A.A., *Firefly Version 7.1G; www http://classic.chem.msu.su/gran/firefly/index.html.*
11. Lee, C., Yang, W., and Parr, R., *Phys. Rev. B*, 1988, vol. 37, p. 785.
12. Schäfer, A., Huber, C. and Ahlrichs, R., *J. Chem. Phys*., 1994, vol. 100, p. 5829
13. *Basis Set Exchange: v1.22. https://bse.pnl.gov/bse/portal.*
14. Eichkorn, K., Weigend, F., Treutler, O., and Ahlrichs, R., *Theor. Chem. Acc*., 1997, vol. 97, p. 119.